Formation and Dissociation of Short-Lived Class II MHC–Peptide Complexes†

Stephan N. Witt‡ and Harden M. McConnell*

Department of Chemistry, Stanford University, Stanford, California 94305

Received August 9, 1993; Revised Manuscript Received November 3, 1993®

ABSTRACT: The incubation of a detergent-solubilized class II MHC protein with excess peptide at 37 °C leads to the formation of long-lived protein–peptide complexes ($\alpha\beta$P*), which have reported dissociation half-times at 37 °C from 30 to 100 h ($\alpha\beta$P* → $\alpha\beta$ + P*). Here we report an unexpected temperature effect on the reaction between class II MHC and added peptide. When the detergent-solubilized mouse class II MHC protein I-A^d is incubated with excess labeled peptide *at 4 °C*, a large fraction of the resultant complexes are relatively short-lived, with dissociation half-times at 40 °C from 2 to 0.2 h. Short-lived complex formation and dissociation are both characterized by nonexponential kinetics. Short-lived I-A^d–peptide complexes may contain two peptides, where the second, added fluorescent peptide is prevented from utilizing all the potential intermolecular interactions in the binding site due to the prior partial occupation of the binding site by a prebound peptide.

Class II MHC[1] molecules are polymorphic, noncovalently associated heterodimeric ($\alpha\beta$) membrane proteins, expressed by the antigen-presenting cells of the immune system such as macrophages, dendritic cells, and B-cells, that serve to bind and display antigenic peptides to helper T-cells (Schwartz, 1985; Townsend & Bodmer, 1989). Each organism possesses a limited number of class II MHC molecules; therefore, a given class II MHC molecule must be able to bind numerous different peptides, with different sequences and lengths. Thus, peptide binding to class II MHC molecules is relatively nonspecific.

A recent X-ray crystal structure of a class II MHC protein (Brown et al., 1993) has revealed that the peptide binding site is structurally similar to the binding site of the related class I MHC proteins (Bjorkman et al., 1987a,b). The class II MHC peptide binding site is a groove formed from the α-subunit and the β-subunit. The groove consists of a β-sheet "floor" that is topped by two parallel α-helices, one from the α-subunit, the other from the β-subunit. The bound peptide lies in the groove between the helices and contacting the β-sheet floor.

Peptide binding to and dissociation from class II MHC proteins is slow (5 h < $t_{1/2}$ < 100 h) (Sette et al., 1992). The kinetic mechanism which governs complex formation and dissociation has not been fully elucidated. Previous kinetic studies of detergent-solubilized class II MHC proteins have shown that the long formation half-times and the low occupation are related to the saturation of the binding sites with endogenous peptides (Buus et al., 1988), which must dissociate prior to the binding of added peptide (Witt & McConnell, 1991). The half-times for the dissociation of a number of related peptides from preformed complexes ($\alpha\beta$P*), prepared at 37 °C, are nearly constant. That is, $t_{1/2}$ is then relatively insensitive to the structure of the peptide (Witt & McConnell, 1992b).

The heterogeneity of isolated class II MHC molecules, that is, whether binding sites are occupied with long or short peptides or with no peptides at all, complicates the interpretion of kinetic data. This is particularly true for complex formation kinetics. In contrast, fluorescent peptide dissociation studies at 37 °C apparently probe one population of protein–peptide complexes since they yield a single exponential decay. We show here that when class II MHC–peptide complexes are prepared at 4 °C, the resultant peptide dissociation kinetics reflect, at least, two subpopulations of class II MHC–peptide complexes. Unlike some of the long-lived complexes prepared at 37 °C, the half-times for peptide dissociation from preformed complexes prepared at 4 °C are sensitive to the peptide's structure. We consider mechanisms that can account for the formation of two different MHC–peptide complexes, depending on the incubation temperature. Since more than one mechanism is possible, our discussion focuses on the simplest possible interpretation of the data. Alternative mechanistic interpretations of the results are given in the Appendix.

MATERIALS AND METHODS

Unless otherwise noted, all chemicals were purchased from Sigma. The OVA peptide (ISQAVHAAHAEINEAGRY) (Tampé & McConnell, 1991), the pCyt*c* peptide (AERADLIAYLKQATAK) Witt & McConnell, 1991), and the HSV peptide (SLKMADPNRFRGKDLP) (Tampé & McConnell, 1991) were prepared as described. Each peptide was fluoresceinated at the N-terminus with either fluorescein isothiocyanate or the succinimidyl ester of fluorescein (Molecular Probes, Eugene, OR). The concentration of labeled peptide was determined spectrophotometrically (λ = 495 nm), using 5-carboxyfluorescein as a standard. The concentration of unlabeled OVA and pCyt*c* was determined at 275 nm, where tyrosine absorbs (ϵ(275 nm) = 1500 M^{-1} cm^{-1}).

A protease inhibitor cocktail was used in some experiments. The final concentration of inhibitors was as follows: PMSF

† Support for this work came from a Stanford University Training Program in Immunology fellowship (AI-07290, S.N.W.) and from a National Institutes of Health grant (5R37 AI13587-17).

* To whom correspondence should be addressed.

‡ Present address: Dept. of Biochemistry & Molecular Biology, Louisiana State University Medical Center, 1501 Kings Highway, Shreveport, LA 71130-3932.

® Abstract published in *Advance ACS Abstracts,* January 15, 1994.

[1] Abbreviations: MHC, major histocompatibility complex; OVA, a peptide representing residues 323–340 of chicken ovalbumin; pCyt*c*, a peptide representing residues 89–104 of pigeon cytochrome *c*; HSV, a peptide representing residues 8–23 of the herpes simplex virus glycoprotein D; HPSEC, high-performance size exclusion chromatography; PMSF, phenylmethanesulfonyl fluoride; EDTA, ethylenediaminetetraacetic acid; TLCK, N^{α}-*p*-tosyl-L-lysine chloromethyl ketone; PBS, phosphate-buffered saline; DM, dodecyl maltoside.

0006-2960/94/0433-1861$04.50/0

(1.2 mM), EDTA (2.7 mM), *N*-ethylmaleimide (6.4 mM), TLCK (0.15 mM), pepstatin A (0.06 mM), and 1.10 phenanthroline (1.1 mM) (Pedrazzini et al., 1991).

HPSEC was used to monitor the population of I-A^d–peptide complexes. The columns separate molecules by molecular weight and readily separate protein–peptide complexes ($\alpha\beta$P*, ~62 kDa) from free fluorescent peptide (P*, ~2 kDa). Columns were purchased from Toso Haas (TSK G3000SW, 7.5 mm × 60 cm). A precolumn was used in all experiments (7.5 mm × 7.5 cm). A single Rainin HPLC pump was used to pump solvent through the columns. The column run-through went through an absorbance detector and fluorescence detector (Gilson Model 121 fluorometer) in series (Witt & McConnell, 1991). The column buffer was PBS/DM (10 mM P_i, 150 mM NaCl, 1.0 mM DM, 0.02% w/v sodium azide, pH 7.0). The column flow rate was 1 mL/min. The amount of fluorescent peptide bound to I-A^d was determined using standard solutions of 5-carboxyfluorescein. The column was maintained at room temperature, 22–23 °C.

The mouse class II MHC protein I-A^d was isolated from A20 hybridomas using an MKD6 monoclonal antibody affinity column as described (Viguier et al., 1990). A20 cells were stored as packed cells at −80 °C prior to lysis. The lysis was conducted using the non-ionic detergent Nonidet-40. Following elution from the affinity column, fractions containing protein were pooled and dialyzed for 24 h at 22 °C against two 500-mL aliquots of PBS/DM. The optical density of detergent-solubilized I-A^d is between 0.1 and 0.2 at 280 nm. Protein determination was conducted by the method of Lowry. The protein was stored at 4 °C prior to use.

When affinity pure I-A^d, which has been stored at 4 °C, is injected on the HPSEC column, two bands are observed in the absorbance-detected chromatograms (V_e = 13.2 and 14.8 mL). The fraction at 14.8 mL is the $\alpha\beta$ heterodimer (Witt & McConnell, 1992a,b). The fraction at 13.2 mL is probably a dimer of heterodimers $(\alpha\beta)_2$. In order to conduct formation kinetic experiments on heterodimeric molecules only, concentrated aliquots of I-A^d were passed down the size exclusion column and the fraction centered at 14.8 mL was collected. All formation kinetic experiments described below used this double purification procedure. See the Appendix, section A, for further discussion.

Peptide binding and dissociation experiments were conducted at pH 5.3 by the addition of an aliquot of concentrated citrate buffer to the protein solution (1 M citrate, pH 4.8) to give a final concentration of 100 mM citrate. Samples were then placed in a thermostated water bath at the desired temperature.

RESULTS

The kinetics of OVA* binding to I-A^d at 37 °C are shown in Figure 1A. The complex formation curves are characterized by the following features. When the concentration of OVA* is increased from 2 to 45 μM, the initial rates of complex formation increase, as expected. At long times (t > 50 h) a gradual reduction in the fluorescence intensity asymptote is observed, especially for samples incubated with a relatively low concentration of peptide. This instability has been extensively analyzed and is due to slow splitting of the heterodimer (see the Appendix, section B). If this gradual reduction at long times is disregarded, each formation curve can be fitted by a single exponential function. After a 150-h incubation of I-A^d with 45 μM OVA*, only 2% of the binding sites are occupied with OVA*. As a negative control, I-A^d was incubated with HSV*. No binding of HSV* to I-A^d is observed at 37 °C, consistent with previous reports (Buus et al., 1987). With respect to the half-times for complex formation, $t_{1/2}$ increases from 3 to 11 h when the peptide concentration is increased from 2 to 45 μM (Figure 1B). A negative slope in the plot of $t_{1/2}$ vs 1/[P*] is consistent with a peptide replacement reaction (eqs 1 and 2) (Witt & McConnell, 1993).

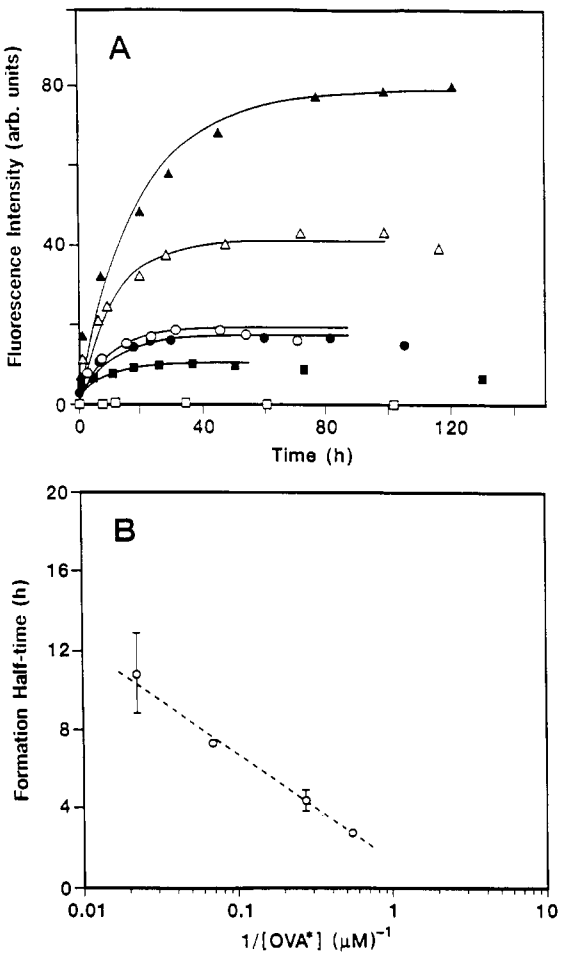

FIGURE 1: The kinetics of OVA* binding to I-A^d at 37 °C (pH 5.3). (A) Complex formation with I-A^d (125 nM) and OVA* at 1.8 (■), 3.6 (○), 14 (△), and 45 μM (▲). One sample contained a protease inhibitor cocktail and 3.6 μM OVA* (●). As a negative control, I-A^d was incubated with the nonbinding peptide HSV* (10 μM, □). Data are fitted to an exponential function (solid lines). (B) A plot of the formation half-time versus 1/[OVA*]. Error bars represent the standard error of the mean (SEM) of duplicates. The dashed line through the data is to help guide the eye.

$$\alpha\beta\text{P} \underset{k_{on}}{\overset{k_{off}}{\rightleftharpoons}} \alpha\beta + \text{P} \quad (1)$$

$$\text{P*} + \alpha\beta \underset{k_{off}}{\overset{k_{on}}{\rightleftharpoons}} \alpha\beta\text{P*} \quad (2)$$

To ascertain whether the gradual reduction in the $\alpha\beta$–OVA* signal is due to proteolysis or to a heterodimer cleavage reaction, a sample of doubly purified I-A^d and OVA* (3.6 μM) was incubated with a protease inhibitor cocktail (see Materials and Methods). The formation curve is shown in Figure 1A. The formation curve has a nearly stable asymptote until 80 h. After 80 h of incubation a gradual reduction in signal is observed. An identical sample without the protease inhibitor cocktail has a nearly stable asymptote until 50 h,

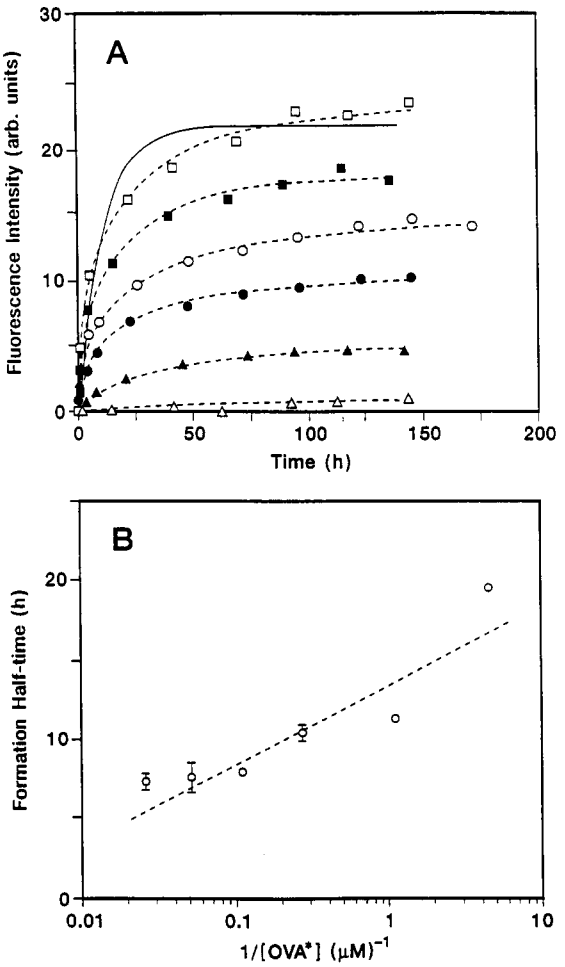

FIGURE 2: The kinetics of OVA* binding to I-A^d at 4 °C (pH 5.3). (A) Complex formation with I-A^d (110 nM) and OVA* at 0.25 (▲), 1.0 (●), 5 (○), 20 (■), and 45 μM (□). As a negative control I-A^d was incubated with the nonbinding peptide HSV* (10 μM, △). The dashed lines through the data are to help guide the eye. The curve, obtained at 45 μM OVA*, is fitted to an exponential function (solid line). (B) A plot of the formation half-time versus 1/[OVA*]. Error bars represent the standard error of the mean (SEM) of duplicates. The dashed line through the data is to help guide the eye.

which is followed by a slight reduction in signal. The two formation curves are nearly superimposable, with nearly identical half-times ($t_{1/2}$ = 4.3 vs 4.5 h). Additionally, the αβ heterodimer signal for each sample was monitored during the incubations using UV absorption (data not shown). The weak αβ heterodimer signal decays with approximately the same rate for each sample. Thus, the gradual reduction in the αβ-OVA* signal at long times and low peptide concentrations in the absence of protease inhibitors is unlikely to be due to proteolysis; it is probably due to a heterodimer cleavage reaction (αβ → α + β, and/or αβP* → αP* + β and α + βP*) (Witt & McConnell, 1992a). See the Appendix, section B, for further discussion of heterodimer cleavage.

The kinetics of OVA* binding to I-A^d at 4 °C are shown in Figure 2A. The molecular complex formation curves are characterized by the following features. When the concentration of OVA* is increased from 0.25 to 45 μM, the initial rates of complex formation increase. The curves reach stable asymptotes after approximately 100 h of incubation at 4 °C. The complex formation curves in Figure 2 cannot be fitted to a single exponential function. Similar to the formation kinetics at 37 °C, the amount of OVA* bound is quite low. After a 7-day incubation with 200 μM OVA* at 4 °C, only 1.6% of the I-A^d binding sites are occupied with OVA*. There is negligible binding of HSV* to I-A^d at 4 °C (Figure 2A). In contrast to the results obtained at 37 °C, when the peptide concentration is increased from 0.25 to 45 μM at 4 °C, the half-time for complex formation decreases from 20 to 7.5 h (Figure 2B). The inverse dependence of the formation half-time on the peptide concentration is consistent with a simple second-order reaction (eq 3 or 4).

$$P^* + \alpha\beta \underset{k_{off}}{\overset{k_{on}}{\rightleftharpoons}} \alpha\beta\text{–}P^* \quad (3)$$

$$P^* + \{\alpha\beta P_x\} \underset{k_{off}}{\overset{k_{on}}{\rightleftharpoons}} \{\alpha\beta P_x\}\text{–}P^* \quad (4)$$

A slight change in temperature alters the dependence of the formation half-time on the peptide concentration. The results suggest that at least two different protein–peptide complexes are produced, depending on the incubation temperature.

Specificity controls were conducted to assess whether the observed binding of labeled peptide to I-A^d at 4 °C is subject to competitive inhibition with unlabeled peptide. The binding of OVA* and pCytc* to I-A^d at 4 °C is specific in that unlabeled OVA and unlabeled pCytc competitively inhibit binding of the labeled peptides (data not shown). Moreover, dynorphin 1–13, a peptide that does not bind to I-A^d (Pedrazzini et al., 1991), does not compete with either OVA* or pCytc*, even at a 100-fold molar excess to labeled peptide.

The results below show that the product of the reaction between peptide and I-A^d at 4 °C is different from the product of the reaction between peptide and I-A^d at 37 °C. I-A^d was incubated with OVA* at pH 5.3 at 4 °C for 5–7 days. Complexes were then separated from free labeled peptide via a brief passage (0.25 h) down a size exclusion column which was maintained at pH 7.0 at 22–23 °C. In all cases, the transit time on the size exclusion column was significantly less than the half-time for peptide dissociation. The fraction containing αβP* complexes was immediately placed on ice. Dissociation kinetic experiments were initiated by a pH-jump (from 7.0 to 5.3) and a T-jump to the desired temperature. For I-A^d–OVA* complexes prepared at 4 °C, the dissociation curves, obtained over a range of temperatures, are shown in Figure 3. Peptide dissociation is biphasic, with a fast phase and a slow phase according to

$$F(t)/F(0) = A\exp(-k_f t) + B\exp(-k_s t) \quad (5)$$

The rate constants and relative amplitudes were determined by fitting the dissociation data to eq 5. (Figure 3, Table 2). (The relative amplitudes of the fast phase vary from approximately 0.7 to 0.1 for T = 40 and 20 °C, respectively.) The rapid rate (k_f) of OVA* dissociation does not vary over 20–40 °C (Table 2); in contrast, over the same temperature range, the slow rate (k_s) of OVA* dissociation increases by a factor of 8. In terms of half-times, $t_{1/2}$ for the rapid and slow phases of OVA* dissociation at 40 °C are 2.2 and 26 h (Table 2). For comparison, for preformed I-A^d–OVA* complexes prepared at 37 °C, peptide dissociation is nearly monophasic with a half-time of 33 h (37 °C) ($k = 5.9 \times 10^{-6}$ s^{-1}) (Figure 3, Table 1).

It is important to note that, for the I-A^d–OVA* complex, the length of preincubation at 4 °C does not affect the relative amplitudes of the fast and slow phases. Concentrated I-A^d was preincubated with 200 μM OVA* at 4 °C (pH 5.3). After a 30-h preincubation period, an aliquot was removed and complexes were separated from free peptide. The

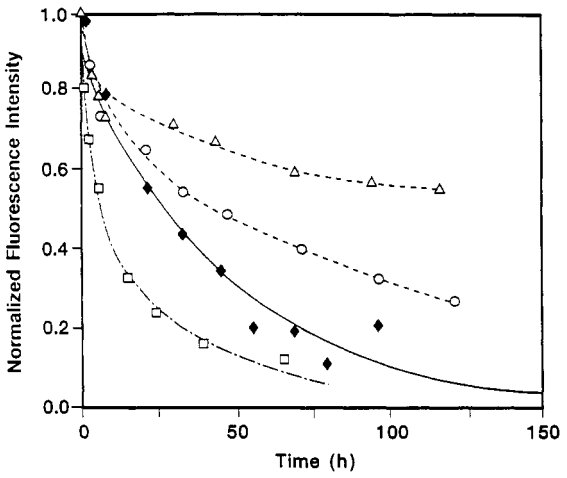

FIGURE 3: Dissociation of OVA* from preformed I-A^d–OVA* complexes prepared at 4 and 37 °C. For preformed complexes prepared at 4 °C, dissociation experiments were conducted at pH 5.3 at 40 (□), 30 (○), and 20 °C (△). All curves were fitted to a double exponential function. (The fitted parameters are given in Table 2). For example, for peptide dissociation at 40 °C, the best fit equation is $F(t)/F(0) = 0.48 \exp[(-8.1 \times 10^{-5}\ s^{-1})t] + 0.49 \exp[(-7.5 \times 10^{-6}\ s^{-1})t]$ (·—·). Otherwise, dashed lines through the data are to help guide the eye. For preformed complexes prepared at 37 °C, a dissociation experiment was conducted at pH 5.3 and 37 °C (♦). The data are fitted to a single exponential function (solid line) ($k = 5.9 \times 10^{-6}\ s^{-1}$).

Table 1: Complexes Prepared at 37 °C. Fits of the Dissociation Kinetic Data to a Single Exponential: $F(t)/F(0) = \exp(-kt)$

	k (s^{-1})	
T (°C)	I-A^d–OVA*	I-A^d–pCyt*c**
20		5.6×10^{-7}
30		7.4×10^{-7}
37	5.9×10^{-6}	
40		2.1×10^{-6}

remaining sample was incubated for 7 days. The dissociation curves for the two samples of preformed complexes are superimposable (observed $t_{1/2} = 7$ h, 40 °C) (data not shown).

The following experiments were conducted to explore the generality of short-lived class II MHC–peptide complexes. I-A^d and pCyt*c** were preincubated for a long time at 4 °C (pH 5.3). The resultant complexes were isolated as described; complexes were subsequently incubated at 30, 20, and 10 °C (pH 5.3). At all temperatures, pCyt*c** dissociation is biphasic (Figure 4). The biphasic dissociation data were fitted to the double exponential (Table 2). (The relative amplitudes of the fast phase vary from approximately 0.5 to 0.6 for $T = 40$ and 20 °C, respectively.) From 10 to 30 °C there is an 11-fold increase in the rapid rate (k_f) of pCyt*c** dissociation (Table 2). In terms of half-times, $t_{1/2}$ for the rapid and slow phases of pCyt*c** dissociation at 30 °C are 0.6 and 120 h. For comparison, for preformed I-A^d–pCyt*c** complexes prepared at 37 °C, peptide dissociation at 30 °C is monophasic ($t_{1/2}$ = 260 h) (Figure 4, Table 1).

Arrhenius plots of the data in Table 2 are given in Figure 5. The activation enthalpy and prefactor are determined from the slope and intercept of the plots, respectively. Since the double exponential represents two discrete subpopulations, two plots are evident for each protein–peptide complex in Figure 5. The slope in the plot of the rapid phase of OVA* dissociation is slightly positive, indicating an observed negative activation enthalpy ($\Delta H^* = -6.3 \pm 0.2 \times 10^{-1}$ kcal/mol and frequency prefactor = $3.4 \pm 0.4 \times 10^{-5}\ s^{-1}$). The activation parameters for the rapid phase of pCyt*c** dissociation are $\Delta H^* = 21.4 \pm 0.1$ kcal/mol and frequency prefactor = $9.7 \pm 2.1 \times 10^{11}\ s^{-1}$. With respect to the slow phase of OVA* dissociation, $\Delta H^* = 18.9 \pm 0.1$ kcal/mol and frequency prefactor = $1.1 \pm 0.1 \times 10^{8}\ s^{-1}$. (Since there are only two rate constants for the slow phase of pCyt*c** dissociation (Table 2), the activation enthalpy and frequency prefactor are not reported.) An Arrhenius plot of the rate constants in Table 1 is also shown in Figure 5. For the dissociation of pCyt*c** from preformed complexes (prepared at 37 °C), the activation enthalpy and frequency prefactor are 12 ± 2 kcal/mol and 440 s^{-1}.

DISCUSSION

We have described an unexpected effect of temperature on the formation of class II MHC–peptide complexes: approximately 50% of the class II MHC–peptide complexes that form at 4 °C are relatively short-lived at elevated temperatures; the remaining complexes are long-lived. The kinetics of short-lived complex formation and dissociation can be interpreted in terms of forward and reverse reaction 4. This reaction is consistent with the formation of both short- and long-lived complexes at low temperatures. As discussed below, this scheme is also consistent with the high-temperature kinetic results.

We first summarize the kinetics of I-A^d–OVA* complex formation at 37 °C, and then the kinetics at 4 °C. For I-A^d–OVA* complex formation at 37 °C, the formation half-time ($t_{1/2}$) decreases from 11.5 to 2 h upon lowering the peptide concentration from 45 to 2 μM (Figure 1B). A decrease in $t_{1/2}$ at low peptide concentrations was also observed for the formation of complexes between pCyt*c** and the mouse class II MHC membrane protein I-E^k at 37 °C (Witt & McConnell, 1991). The origin of the effect has been discussed at length (Witt & McConnell, 1993). A negative slope in the plot of $t_{1/2}$ vs $1/[P^*]$ is consistent with complex formation via a peptide replacement reaction (eqs 1 and 2). For example, if forward reaction 2 is fast and the initial concentration of added peptide is much greater than the concentration of protein, then the formation reaction goes to completion with a half-time equal to the half-time for peptide dissociation ($t_{1/2}$(formation) = $(\ln 2)/k_{off}$). In contrast, if the concentration of added peptide is less than that of the protein, only a small fraction of binding sites have to become unoccupied for forward reaction 2 to consume one-half of the concentration of added peptide. Clearly, the half-time for complex formation under such conditions can be much less than $(\ln 2)/k_{off}$. In the earlier work on I-E^k, it was also found that the half-times for the dissociation of labeled peptide from preformed I-E^k–pCyt*c** complexes are nearly identical to the half-times for complex formation. These two features indicate that complex formation is due to a peptide replacement reaction. For I-A^d–OVA* complex formation at 37 °C, the decrease in $t_{1/2}$ at low peptide concentrations is consistent with complex formation via peptide replacement.

The kinetics of complex formation at 4 °C and the kinetics of peptide dissociation from preformed complexes (prepared at 4 °C) exhibit some features which have been observed previously at higher temperatures, and others that are distinctly different. It is useful to summarize these features. (i) The low level of peptide binding at 4 °C (1.6%) is similar to the level of binding at 37 °C (2%); (ii) labeled peptide binding to I-A^d at 4 °C is subject to competitive inhibition with unlabeled peptide; (iii) complex formation at 4 °C is nonexponential (Figure 2A); (iv) the formation half-time has an inverse dependence on peptide concentration (Figure 2B);

Table 2: Complexes Prepared at 4 °C. Fits of the Dissociation Kinetic Data to a Double Exponential: $F(t)/F(0) = A \exp(-k_f t) + B \exp(-k_s t)$[a]

	I-A^d–OVA*		I-A^d–pCyt*c*	
T (°C)	k_f (s^{-1})	k_s (s^{-1})	k_f (s^{-1})	k_s (s^{-1})
10			2.8×10^{-5}	poor fit
20	$9.4 \pm 0.5 \times 10^{-5}$	$9.3 \pm 0.7 \times 10^{-7}$	$1.5 \pm 0.5 \times 10^{-4}$	$8.4 \pm 0.6 \times 10^{-7}$
30	$1.0 \pm 0.1 \times 10^{-4}$	$2.8 \pm 0.4 \times 10^{-6}$	$3.3 \pm 0.8 \times 10^{-4}$	$1.6 \pm 0.1 \times 10^{-6}$
40	$8.8 \pm 0.4 \times 10^{-5}$	$7.4 \pm 1.3 \times 10^{-6}$		

[a] The uncertainties in rate constants are the SEM of duplicates.

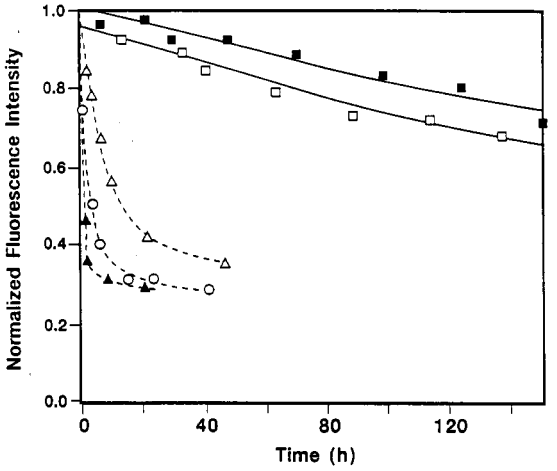

FIGURE 4: Dissociation of pCyt*c** from preformed I-A^d–pCyt*c** complexes prepared at 4 and 37 °C. For preformed complexes prepared at 4 °C, dissociation experiments were conducted at pH 5.3 at 30 (▲), 20 (○), and 10 °C (△). Dashed lines through the data are to help guide the eye. Each curve was fitted to a double exponential (Table 2). For preformed complexes prepared at 37 °C, dissociation experiments were conducted at pH 5.3 at 30 (□) and 20 °C (■). The data are fitted to a single exponential function (solid lines) (Table 1).

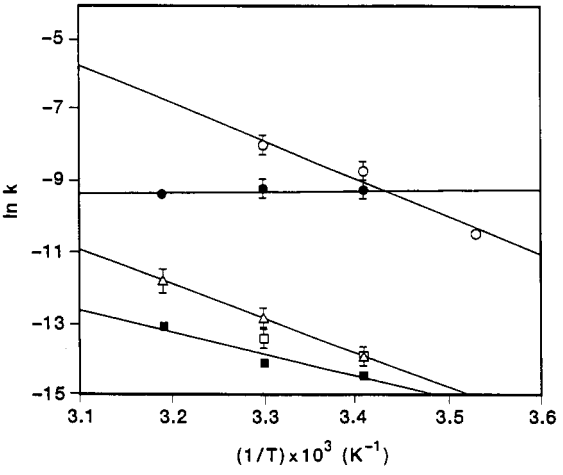

FIGURE 5: Arrhenius plots. Rate constants from Table 2: ●, rapid phase of OVA* dissociation, $\Delta H^* = -6.3 \pm 0.2$ kcal/mol, frequency prefactor = $3.4 \pm 0.4 \times 10^{-5}$ s^{-1}; ○, rapid phase of pCyt*c** dissociation, $\Delta H^* = 21.4 \pm 0.1$ kcal/mol, frequency prefactor = $9.7 \pm 2.1 \times 10^{11}$ s^{-1}; △, slow phase of OVA* dissociation, $\Delta H^* = 18.9 \pm 0.1$ kcal/mol, frequency prefactor = $1.1 \pm 0.1 \times 10^8$ s^{-1}; □, slow phase of pCyt*c** dissociation (two points). Rate constants from Table 1: ■, OVA* dissociation, $\Delta H^* = 12 \pm 2$ kcal/mol, frequency prefactor = 440 ± 20 s^{-1}.

and (v) peptide dissociation from preformed complexes (prepared at 4 °C) is biphasic, with a rapid and a slow phase.

To interpret the above results, let us assume that at the onset of a kinetic experiment approximately 90% of the class II MHC binding sites are occupied with long endogenous peptides (which might prevent the binding of a second, added peptide), a small fraction of the sites are occupied with short endogenous peptides (which allow the binding of a second, added peptide), and a small fraction of the sites are empty. (Peptides as short as five amino acids are known to bind to class II MHC proteins with long life times. See Dornmair et al., 1991.) Biphasic formation and dissociation kinetics are expected at low temperatures with such initial conditions. That is, upon addition of peptide the sites with short peptides react with k'_{on} and k'_{off} to form short-lived, two-peptide complexes; the unoccupied sites react with k_{on} and k_{off} to form long-lived, one-peptide complexes $\alpha\beta$P* (where $k_{on} \gg k'_{on}$ and $k_{off} \ll k'_{off}$). At elevated incubation temperatures, we expect that usually only a one-peptide complex is present due to the relative instability of the two-peptide complex. Further, if prebound short peptides dissociate at elevated temperatures, empty sites then react with added peptides to form long-lived complexes $\alpha\beta$P*. The observed decrease in $t_{1/2}$ at low peptide concentrations at 37 °C (Figure 1B) is consistent with such a peptide replacement reaction. The kinetics of complex formation (and peptide dissociation) in the high- and low-temperature regimes can be understood qualitatively in terms of forward and reverse reaction 4.

Since the life-time of the two-peptide complex is sensitive to the structure of the peptide, in some cases, a two-peptide complex may persist long enough at elevated temperatures to be detected. In earlier work, it was shown that two-peptide class II MHC complexes do persist long enough to be detected, even in the presence of low concentrations of sodium dodecyl sulfate (Tampé et al., 1991).

In conclusion it may also be noted that in selected cases there is kinetic evidence that two peptide complexes can function as reaction intermediates in the displacement of one bound peptide by another (de Kroon & McConnell, 1993). This accumulating evidence for two-peptide complexes with class II MHC molecules raises the possibility that they may sometimes have functional significance.

ACKNOWLEDGMENT

We are indebted to Dr. Dan Denney for helpful discussions.

APPENDIX

Both the execution and interpretation of the work described in this paper involve a number of ancillary technical issues that are summarized in this Appendix.

A. Dimerization of I-A^d. When an aliquot of relatively concentrated I-A^d (2 μM) is injected on the size exclusion column, two overlapping bands are usually observed in the absorbance-detected chromatograms (V_e = 13.2 and 14.8 mL) (Figure 6a). When the fractions are collected, concentrated, and subjected to SDS polyacrylamide electrophoresis without boiling or reducing, each fraction yields a four-band pattern consisting of "floppy" and "compact" heterodimers and β and α subunits (data not shown). (For the class II MHC protein I-E^k, which was typically used at lower concentrations (0.1–0.2 μM), the absorbance-detected chromatograms consisted of one band (V_e = 14.8–15 mL), the $\alpha\beta$ heterodimer band.)

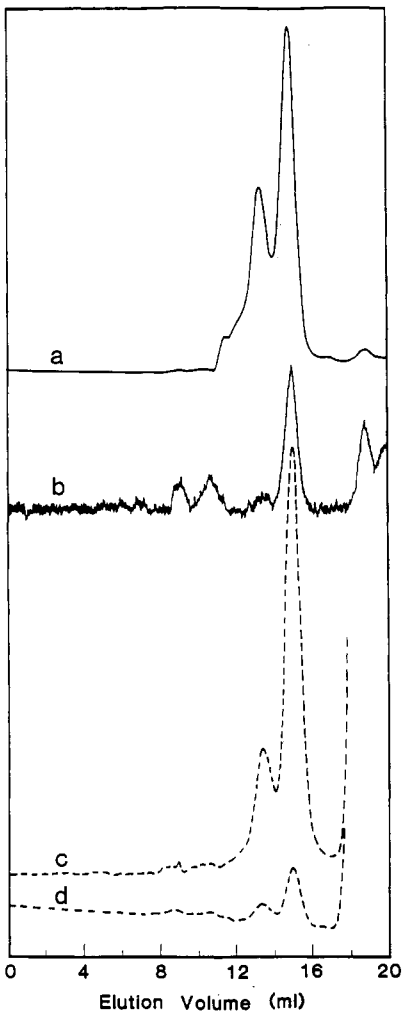

FIGURE 6: Dimerization of I-A^d. Absorbance-detected (solid lines) and fluorescence-detected (dashed lines) chromatograms of I-A^d with and without OVA*. (a) Injection of 23 μg of affinity pure I-A^d. (b) The fraction at 14.8 mL was collected, diluted, and reinjected (0.5 μg). (c) After I-A^d (0.25 μM) and OVA* (1 μM) were incubated for 3 days at 4 °C, an aliquot (0.75 μg) was injected. (d) An identical sample with a 25-fold molar excess of unlabeled OVA.

A reasonable explanation of the two bands is that I-A^d dimerizes ($2\alpha\beta \rightarrow (\alpha\beta)_2$); thus the fraction at 13.2 mL is $(\alpha\beta)_2$. To conduct formation kinetic experiments without contamination from the dimer, aliquots of I-A^d were passed over the size exclusion column and the $\alpha\beta$ fraction was collected. An approximately 10-fold dilution of the protein occurs upon passage through the column. No significant dimer re-formation was observed upon reinjection (Figure 6b).

The dimer of heterodimers binds fluorescent peptide (Figure 6c). The incubation of I-A^d with OVA* at 4 °C results in the formation of bands in the fluorescence-detected chromatograms at 13.2 and 14.8 mL. This is consistent with the formation of $\alpha\beta$P* and $(\alpha\beta$P*$)_2$. The binding of OVA* to both species is subject to competitive inhibition with unlabeled OVA ([OVA]/[OVA*] = 25) (Figure 6d). When the fraction containing $(\alpha\beta$P*$)_2$ complexes is collected and then reinjected, a less intense band is observed at the original position (13.2 mL). However, if the $(\alpha\beta$P*$)_2$ fraction is incubated at 37 °C, there is a gradual reduction in intensity of the band at 13.2 mL, with a concomitant growth in intensity of the band at 14.8 mL. This result is consistent with deaggregation [$(\alpha\beta$P*$)_2 \rightarrow 2\alpha\beta$P*]. Wiley and co-workers have recently shown that a soluble version of the human class II MHC protein DR-1 crystallizes as a dimer (Brown et al., 1993).

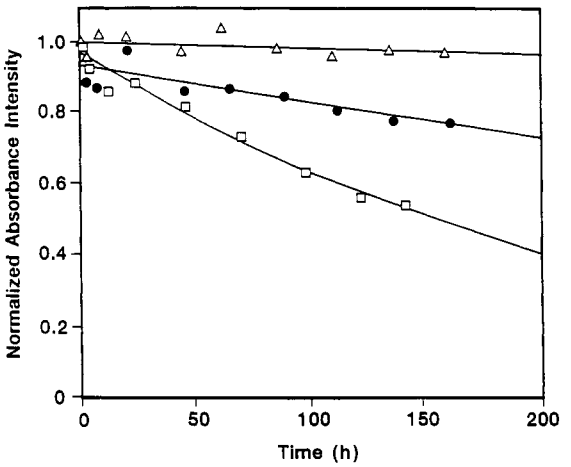

FIGURE 7: Heterodimer cleavage. Heterodimer cleavage kinetics were conducted at 40 (□), 30 (●), and 20 °C (△) at pH 5.3. Data are fitted to a single exponential (solid lines). First-order rate constants are 1.2×10^{-6} s^{-1} (40 °C), 3.3×10^{-7} s^{-1} (30 °C), and 5×10^{-8} s^{-1} (20 °C).

B. Heterodimer Cleavage Kinetics ($\alpha\beta \rightarrow \alpha + \beta$). Heterodimer cleavage was monitored by periodically injecting purified I-A^d on a size exclusion column and following the diminution in intensity of the $\alpha\beta$ absorption signal (V_e = 14.8 mL) at 280 nm. Proteolysis and nonspecific sticking of the protein to the wall of the sample tube might also reduce the population of $\alpha\beta$ heterodimers. Proteolysis is ruled out on the basis of the experiments described above; nonspecific sticking is ruled out as described (Witt & McConnell, 1992a,b). The kinetic curves for the heterodimer cleavage reaction are shown in Figure 7. It is important to note that there is a rapid loss of $\alpha\beta$ signal (~10%) that occurs within approximately 5 h for $T > 20$ °C. The small subpopulation may be the active heterodimers, which are prone to rapid cleavage because the binding sites are empty or occupied with more rapidly dissociating endogenous peptides. The large subpopulation (90%) of I-A^d $\alpha\beta$ heterodimers is remarkably resistant to cleavage, probably because the binding sites are occupied with tightly bound endogenous peptides. The first-order rate constants for cleavage are 1.2×10^{-6} s^{-1} (40 °C), 3.3×10^{-7} s^{-1} (30 °C), and 5×10^{-8} s^{-1} (20 °C). The activation enthalpy and frequency prefactor are 29 kcal/mol and 1.4×10^{14} s^{-1}, respectively.

C. Analysis of the Nonexponential Kinetic Curves. Many of the kinetic data in the present study can be accounted for in terms of a power law, corresponding to a spectrum of rate constants.

$$F(t)/F(0) = (1 + t/t_0)^{-n} \quad (6)$$

There is a simple relationship between the most probable rate constant (k_p) in the distribution and the parameters n and t_0, that is, $k_p = n/t_0$, where $0 < n < 1$. For a discussion of the use of the power law to interpret chemical kinetics, see Austin et al. (1974) and Agmon and Hopfield (1983).

The power law can be used to analyze both the nonexponential dissociation and formation curves. The use of the power law for peptide dissociation is justified if two-peptide complexes $\{\alpha\beta P_x\}$–P* (eq 4) have off rates that are heterogeneous, that is, rates that depend on the length of the prebound peptide. The parameters n and t_0 were determined by fitting dissociation kinetic data to eq 6. The most probable dissociation rate constants are given in Table 3. As an example, for the dissociation of OVA* at 40 °C (from preformed

Table 3: Complexes Prepared at 4 °C. Fits of the Dissociation Kinetic Data to a Power Law: $F(t)/F(0) = (1 + t/t_0)^{-n}$

T (°C)	I-A^d–OVA*: k_p[a] (s^{-1})	I-A^d–pCyt$c$*: k_p (s^{-1})
10		2.6×10^{-5}
20	$4.2 \pm 1.0 \times 10^{-5}$	$1.6 \pm 0.1 \times 10^{-4}$
30	$1.3 \pm 0.1 \times 10^{-5}$	$4 \bullet 3 \times 10^{-3}$
40	$4.4 \pm 1.0 \times 10^{-5}$	

[a] The most probable rate constant in the distribution is given by $k_p = n/t_0$ (±SEM).

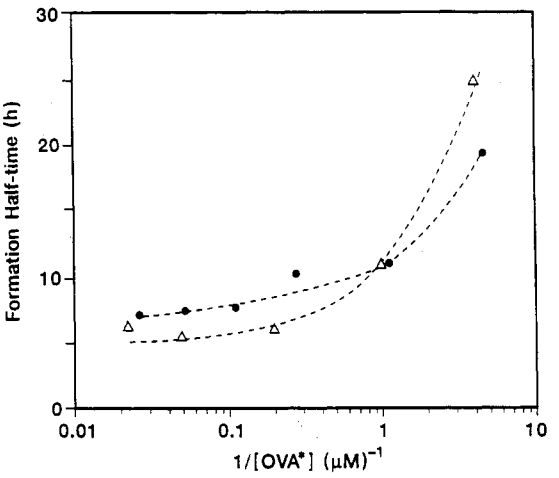

FIGURE 8: Power law fit of the nonexponential formation kinetic data. The formation curves in Figure 2 were fitted to eq 8. The fitted formation half-times [(ln2)t_0/n] (△) and the observed formation half-times (●) (Figure 2B) are plotted versus 1/[P*].

complexes prepared at 4 °C) (Figure 3), the best fit to the power law is

$$F(t)/F(0) = (1 + t/(3.6\text{ h}))^{-0.69} \quad (7)$$

$$k_p(\text{s}^{-1}) = \frac{0.69}{3.6\text{ h}}\frac{1\text{ h}}{3600\text{ s}} = 5.3 \times 10^{-5}\text{ s}^{-1}$$

In every case, the dissociation data can be fitted by the two-parameter power law as well as (or better than) the double exponential, which has four parameters.

Using the data in Table 3, an Arrhenius plot was made. The most probable activation enthalpy (ΔH_p^*) and the frequency prefactor for the reaction $\alpha\beta$–OVA* → $\alpha\beta$ + OVA* are 0.5 ± 0.3 kcal/mol and $6 \pm 4 \times 10^{-5}$ s^{-1}, respectively. The most probable activation enthalpy and the frequency prefactor for the reaction $\alpha\beta$–pCyt$c$* → $\alpha\beta$ + pCyt$c$* are 43.3 ± 0.2 kcal/mol and $5.6 \pm 2.3 \times 10^{28}$ s^{-1}, respectively.

The power law can also be used to analyze the nonexponential complex formation curves. We assume that the formation kinetics at 4 °C reflect a distribution of on rates. Further, the formation experiments were carried out with [P*] ≫ $[\alpha\beta]_0$, so that the reaction is pseudo-first-order. The complex formation curves obtained at 4 °C were fitted to

$$F(t) = F(\infty)[1 - (1 + t/t_0)^{-n}] \quad (8)$$

As an example, complex formation with 45 μM OVA* at 4 °C (Figure 2A) follows

$$F(t) = 58.7[1 - (1 + t/(0.88\text{ h}))^{-0.1}] \quad (9)$$

The half-times obtained from the power law fits are nearly identical to the observed half-times for complex formation at 4 °C (Figure 8). The nonexponential kinetic data are thus consistent with a distribution of protein–peptide kinetic rate constants.

D. Sequential Kinetics. In previous work we found that three related ovalbumin peptides dissociate from preformed I-A^d complexes (prepared at 37 °C) with a 100-h half-time (37 °C, pH 5.3) (Witt & McConnell, 1992b). The OVA peptides used in this earlier work contained a lysine residue at position 339. The pigeon cytochrome c peptide (pCyt$c$*-(89–104)), which has a sequence unrelated to OVA, also dissociates from preformed complexes with a 100-h half-time (37 °C, pH 5.3). Here we report that OVA*(323–339)Y, where position 339 is an arginine residue, dissociates from complexes prepared at 37 °C with a half-time of 33 h (37 °C, pH 5.3). Thus, changing position 339 from a lysine to an arginine results in a 3-fold reduction in the dissociation half-time.

The near constancy of the dissociation half-time raises the possibility that the reaction follows a sequential mechanism,

$$\{\alpha\beta\text{P}^*\}_c \rightleftharpoons \{\alpha\beta\text{P}^*\}_o \quad (10)$$

$$\{\alpha\beta\text{P}^*\}_o \rightleftharpoons \{\alpha\beta\}_o + \text{P}^* \quad (11)$$

where o and c refer to protein structures that are "open" and "closed". Reactions 10 and 11 are then sequential reactions, and $\{\alpha\beta\text{P}^*\}_o$ can be regarded as a reaction intermediate (Witt & McConnell, 1993).

Consider class II MHC–peptide complex formation according to the two-step sequential reaction, where short-lived complexes $\{\alpha\beta\text{P}^*\}_o$ are in equilibrium with long-lived complexes $\{\alpha\beta\text{P}^*\}_c$. For this reaction, we must assume that only the long-lived molecular complex $\{\alpha\beta\text{P}^*\}_c$ is populated at elevated temperatures ($T \geq 37$ °C), whereas both complexes ($\{\alpha\beta\text{P}\}_c$ and $\{\alpha\beta\text{P}\}_o$) are populated at low temperatures ($T \leq 4$ °C). The observed biphasic dissociation kinetics, for preformed complexes prepared at 4 °C, indicate that two subpopulations of molecular complexes form at low temperatures. (One subpopulation of complexes is short-lived; the other subpopulation is long-lived.) In general, the half-times for the short-lived species are 6–100 times shorter than the half-times of the long-lived species (Table 2). We note that the slow phase of pCyt$c$* dissociation from preformed complexes (prepared at 4 °C) (two points in Figure 5, Table 2) is nearly superimposable on the slow phase of pCyt$c$* dissociation from preformed complexes prepared at 37 °C (Figure 5, Table 1). Likewise, the rate constant for the slow phase of OVA* dissociation ($k = 7.4 \times 10^{-6}$ s^{-1}, 40 °C, Table 2) is nearly the same as the rate constant for the monophasic OVA* dissociation from preformed complexes prepared at 37 °C ($k = 5.9 \times 10^{-6}$ s^{-1}, 37 °C, Table 1). The long-lived complexes that form at low temperatures must be the same as those that form at high temperatures. The peptide dissociation results described above are thus consistent with complex formation via the two-step sequential reaction.

The issue is whether this two-step sequential reaction can account for the *formation* kinetic results at both low and high temperatures. We have simulated the sequential reactions for the case where reverse reaction 11 is slow, and we find that the slope in the plot of $t_{1/2}$ versus 1/[P*] is positive. When reverse reaction 11 is rapid and reverse reaction 10 is slow, the slope in the plot of $t_{1/2}$ versus 1/[P*] is slightly positive, nearly 0. However, a set of rate constants could not be found which results in a decrease in the formation half-time at low peptide concentrations. Thus, the sequential reaction scheme (P* + $\{\alpha\beta\}_o$ → $\{\alpha\beta\text{P}^*\}_o$ → $\{\alpha\beta\text{P}^*\}_c$) cannot account for the observed formation kinetics at 4 and 37 °C, without additional assumptions. However, in the presence of prebound peptides,

we can anticipate that the sequential mechanism would also be consistent with the observed data. In fact, virtually any model in which there is a variety of prebound peptides with different off rates can yield a $t_{1/2}$ vs $1/[P^*]$ plot with negative slope.

REFERENCES

Agmon, N., & Hopfield, J. J. (1983) *J. Chem. Phys. 79*, 2042–2053.

Austin, R. H., Beeson, K., Eisenstein, L., Frauenfelder, H., Gunsalus, I. C., & Marshall, V. P. (1974) *Phys. Rev. Lett. 32*, 403–405.

Bjorkman, P. J., Saper, M. A., Samraoui, B., Bennett, W. S., Strominger, J. L., & Wiley, D. C. (1987a) *Nature 329*, 506–512.

Bjorkman, P. J., Saper, M. A., Samraoui, B., Bennett, W. S., Strominger, J. L., & Wiley, D. C. (1987b) *Nature 329*, 512–518.

Brown, J. H., Jardetzky, T. S., Gorga, J. C., Stern, L. J., Urban, R. G., Strominger, J. L., & Wiley, D. C. (1993) *Nature 364*, 33–39.

Buus, S., Sette, A., Colon, S. M., Miles, C., & Grey, H. M. (1987) *Science 235*, 1353–1358.

Buus, S., Sette, A., Colon, S. M., & Grey, H. M. (1988) *Science 242*, 1045–1047.

De Kroon, A. I. P. M., & McConnell, H. M. (1993) *Proc. Natl. Acad. Sci. U.S.A. 90*, 8797–8801.

Dornmair, K., Clark, B. R., & McConnell, H. M. (1991) *FEBS Lett. 294*, 244–246.

Pedrazzini, T., Sette, A., Albertson, M., & Grey, H. M. (1991) *J. Immunol. 146*, 3496–3501.

Schwartz, R. H. (1985) *Annu. Rev. Immunol. 3*, 237–261.

Sette, A., Southwood, S., O'Sullivan, D., Gaeta, F. C. A., Sidney, J., & Grey, H. M. (1992) *J. Immunol. 148*, 844–851.

Tampé, R., & McConnell, H. M. (1991) *Proc. Natl. Acad. Sci. U.S.A. 88*, 4661–4665.

Tampé, R., Clark, B. R., & McConnell, H. M. (1991) *Science 254*, 87–89.

Townsend, A., & Bodmer, H. (1989) *Annu. Rev. Immunol. 7*, 601–624.

Viguier, M., Dornmair, K., Clark, B. R., & McConnell, H. M. (1990) *Proc. Natl. Acad. Sci. U.S.A. 88*, 7170–7174.

Witt, S. N., & McConnell, H. M. (1991) *Proc. Natl. Acad. Sci. U.S.A. 88*, 8164–8168.

Witt, S. N., & McConnell, H. M. (1992a) *J. Am. Chem. Soc. 114*, 3506–3511.

Witt, S. N., & McConnell, H. M. (1992b) *J. Am. Chem. Soc. 114*, 9680–9682.

Witt, S. N., & McConnell, H. M. (1993) *Acc. Chem. Res. 26*, 442–448.